Constraints on early Cambrian carbon cycling from the duration of the Nemakit-Daldynianian–Tommotian boundary $\delta^{13}C$ shift, Morocco

Adam C. Maloof, Jahandar Ramezani, Samuel A. Bowring,
David A. Fike, Susannah M. Porter, Mohamed Mazouad

GSA Data Repository

DR1 Methods

DR1.1 $\delta^{13}C$

We conducted a program of targeted mapping and physical stratigraphy, with the particular goal of generating a continuous stratigraphic section spanning the ND—T transition and correlative with our previous work, in order to assess lateral isotopic variability across the Anti-Atlas margin. The new Sidi M'Sal section is located 12 km northeast of Tafraoute on the east flank of the Kerdous Inlier (Fig. 1), where the complete early Cambrian platform succession of Morocco is tilted and beveled into a series of ridges that provided nearly 100% exposure of 2.3 km of carbonate sediment (Fig. 2). We sampled the entire succession at 0.5 m resolution while measuring stratigraphic sections. Clean dolostones and limestones without siliciclastic components or secondary veining or cleavage were targeted. Samples were slabbed and polished perpendicular to bedding and $\sim$5 mg of powder were micro-drilled from individual laminations for isotopic analysis. $\delta^{13}C$ and $\delta^{18}O$ compositions were acquired simultaneously on a VG Optima dual inlet mass spectrometer attached to a VG Isocarb preparation device in the Stable Isotope Laboratory at the University

of Michigan. Approximately 1 mg aliquots of powder were reacted in a common, purified H_3PO_4 bath at 90°C for 8-10 minutes. Evolved CO_2 was purified and collected cryogenically, and then analyzed against an in-house reference gas. The analytical uncertainty (1σ) of this measurement was less than $\pm 0.05‰$ for $\delta^{13}C$. Samples were calibrated to VPDB (Pee Dee Belemnite) using six measurements of the Cararra Marble standard for each run of 54 samples. Memory effect associated with the common acid bath system was minimized by increasing the reaction time for dolomite samples and monitoring the measured values of standards. Examination of the variation in standards after each run showed that the error due to memory effect was always $<0.2‰$.

DR1.2 U-Pb. Geochronology

Zircons were separated from crushed samples by standard Wilfley table, magnetic and heavy liquids techniques and hand-picked for clarity and purity under a binocular microscope. For most analyses, zircons were pre-treated using a modification of Mattinson's (Mattinson, 2005) technique of coupled annealing and multi-step digestion (chemical abrasion). In the chemical abrasion method, high temperature annealing repairs radiation damage in zircon and prevents preferential leaching of Pb relative to U during multi-step digestions. Annealed zircons were dissolved in two steps with the initial HF digestion step preferentially dissolving the most damaged zircon most likely to be affected by post-crystallization Pb loss, isolating the highest quality low-U zircon for final analysis. Pre-treated grains were spiked with a mixed ^{205}Pb-^{233}U-^{235}U tracer solution and dissolved in HF. Dissolved Pb and U were separated using an HCl-based ion exchange chemistry procedure (modified after (Krogh, 1973)), loaded onto single, degassed Re filaments together with a silica gel-H_3PO_4 emitter, and their isotopic compositions were measured on the VG Sector 54 thermal-ionization mass spectrometer at the Massachusetts Institute of Technology. More detailed descriptions of analytical prodedures can be found in Ramezani et al. (2007). Isotopic data from four tuffs along with details of fractionation and blank corrections appear in Table S1. The U-Pb data reduction and calculation of ages and their internal uncertainties follow in general the error propagation algorithms of Ludwig (1980) and the program Isoplot (Ludwig, 2005) using the U decay constants of Jaffey et al. (1971). Calculated U-Pb dates are reported at 95% confidence level as summarized in Table S1 and plotted on standard concordia plots of Figure 3. In this study we use two different but intercalibrated tracer solutions (MIT 1L and EARTHTIME 535) and there is

no systematic age bias for zircons in the same sample using both tracers.

We calculate and report $^{206}Pb/^{238}U$, $^{207}Pb/^{235}U$ and $^{207}Pb/^{206}Pb$ dates for each sample (Table DR1) based on coherent clusters of data for which all scatter can be explained by analytical uncertainty alone. Most high-precision zircon data exhibit a slight but systematic discordance (with $^{206}Pb/^{238}U < ^{207}Pb/^{235}U < ^{207}Pb/^{206}Pb$ dates) likely related to inaccuracy in one or both of the U decay constants (Mattinson, 2000; Schoene et al., 2006). We consider the weighted mean $^{206}Pb/^{238}U$ date to be the most precise and accurate representation of the eruption/depositional age.

All calculated age uncertainties are reported as X/Y/Z in Tables 1 and S1, where X is the internal (analytical) uncertainty in the absence of all external or systematic errors, Y incorporates the U-Pb tracer calibration error and Z includes the latter as well as the decay constant errors of Jaffey et al. (Jaffey et al., 1971). The external uncertainties must be taken into account if the results are to be compared with dates obtained in other laboratories or dates derived from other isotopic systems (e.g., $^{40}Ar/^{39}Ar$). For the purposes of calculating rates and durations in the Moroccan early Cambrian, the tracer and decay constant uncertainties can be ignored. Only the internal errors are reported in Figures 2 and 3 and discussed in the following section.

DR2 Results

DR2.1 Carbonate diagenesis

The water/rock ratio in fluids responsible for meteoric diagenesis and metamorphism of carbonate rocks is high with respect to oxygen but low with respect to carbon. Therefore, altered specimens that show severe oxygen-isotope depletion still may faithfully record the $\delta^{13}C$ of oceanic dissolved inorganic carbon (DIC) (Banner and Hanson, 1990). However, work in late Cenozoic carbonates from the Great Bahama Bank (Swart and Eberli, 2005; Swart, 2008) suggests that even $\delta^{13}C$ can be shifted toward more negative values through diagenetic interactions with coastal pore fluids charged in isotopically depleted organic carbon. Knauth and Kennedy (Knauth and Kennedy, 2009) recently proposed covariation in $\delta^{13}C$ and $\delta^{18}O$ as an index for differentiating between pristine and adulterated $\delta^{13}C$ values in altered samples.

In the Taroudant and Tata Groups, lower $\delta^{13}C$ values are not necessarily associated with lower $\delta^{18}O$. In fact, there is no statistically significant covariation between $\delta^{13}C$ and $\delta^{18}O$, whether carbon and oxygen are compared between stratigraphic sections (Fig. **??**A) or by mineralogy and lithofacies (Fig. DR1B). The ND—T transition is characterized by a 9‰ drop in $\delta^{13}C$ over 50-200 meters (Fig. 2). The $\delta^{13}C$ drop is truly a shift to a new regime (rather than an excursion or an anomaly), from a hierarchy of high amplitude positive excursions with peaks of 7‰ in the Nemakit-Daldynian to the low amplitude variability and mean values of -2 to -3‰ in the Tommotian (Fig. 2). No sympathetic negative $\delta^{18}O$ shift is observed across the ND—T boundary. Instead, $\delta^{18}O$ varies chaotically between -5‰ and -8‰ throughout the entire Taroudant Gp, with no significant correlation to $\delta^{13}C$ or lithofacies (Maloof et al., 2005).

Along the axis of the Tiout-Aguerd trough (Fig. 1; MS7: Oued Sdas), the ND—T transition is contained within a thick package of dolomite stromatolites and microbialites (Fig. 2). $\delta^{13}C$ values show no lithological dependence, and in fact, the major lithological transition to the Lie de Vin Fm occurs 75 m above the end of the $\delta^{13}C$ shift (Fig. 2). In contrast, the western (Fig.1; MS16: M'Sal) and eastern (Fig.1; MS11: Bougzoul) edges of the Tiout-Aguerd trough depict an ND—T transition contained within finely interbedded m-scale parasequences of marlstone, wavy-laminated dolosiltite, and dolomite grainstone. In $\sim$25% of cases, dolomite grainstones are 1-2‰ heavier in $\delta^{13}C$ than adjacent wavy laminated dolosiltite (no such pattern is present in $\delta^{18}O$). This lithological influence on $\delta^{13}C$ accounts for the increased scatter toward lighter $\delta^{13}C$ in Sidi M'Sal and Zawyat n' Bougzoul, and may represent the kind of progressive depletion in ^{13}C seen today in Florida Bay as aging water masses on the interior of the shelf accumulate ^{12}C from respired marine organic matter (Patterson and Walter, 1994). On an even finer scale, frequent subaerial exposure surfaces representing 0-50 cm of base level change are associated with brecciated and recrystallized dolostones, but are not systematically depleted in $\delta^{13}C$.

DR2.2 Tuffs

The upper Adoudounian Fm tuffs reported here represent two of at least twenty different 10-60 cm thick, green tuffs speckled with euhedral feldspar phenocrysts. The Lie de Vin Fm tuffs represent two of at least five different 5-160 cm thick, white marly tuffs. All the tuffs examined so far from Oued Sdas contain a dominant population of large (150-400 μm long) and doubly terminated

zircons interpreted to be derived from the volcanic source of the ash.

M223 is a 60 cm thick tuff within a 25 meter thick buildup of stromatolite and microbialite containing at least three tuffs at a stratigraphic height of 614 m in Oued Sdas. We reported an age of 525.38±0.46 Ma for M223 based on single zircon analyses of five air-abraded and three chemically-abraded crystals Maloof et al. (2005). Here, we refine this age with three additional chemically-abraded zircon analyses. Six air-abraded grains and six chemically abraded grains form a cluster with a weighted mean $^{206}Pb/^{238}U$ date of 525.343±0.088 Ma (MSWD = 0.33), which we interpret as the eruption/depositional age (Table DR1). The increase in precision reflects the additional analyses and new spike calibration and should supercede the date published in Maloof et al. (2005). It is noteworthy that the air-abraded grains from this sample yield ages identical to those subjected to chemical abrasion and that there is no difference in dates using two different tracer solutions over 4 years.

M231 is a 50 cm thick tuff within a 14.7 meter thick microbialite in Oued Sdas at a stratigraphic height of 764 m. In this sample, five air-abraded and three chemically-abraded grains form a cluster with a weighted mean $^{206}Pb/^{238}U$ date of 524.837±0.092 (MSWD = 0.72), which we interpret as the eruption/depositional age (Table DR1).

M234 is a 10 cm thick tuff within an 80 cm thick microbialite in Oued Sdas at a stratigraphic height of 1031 m. In this sample, eleven grains subjected to chemical-abrasion (Table DR1) and ten form a cluster with a weighted mean $^{206}Pb/^{238}U$ date of 523.17±0.16 Ma with a MSWD of 1.2 Ma, which we interpret as the age of eruption/deposition. One zircon analysis is distinctly older with a $^{207}Pb/^{206}Pb$ date of 531.6±8.0 Ma and a $^{206}Pb/^{238}U$ date of 523.92±0.07. We interpreted this zircon to show subtle inheritance and we excluded it from the weighted mean.

M236 is a 5 cm thick tuff within a 2.2 meter thick thrombolite bioherm at a stratigraphic height of 1536 m in Oued Sdas. This tuff is located at approximately the same stratigraphic level (±25 m) as the tuff reported a decade ago from Tiout with a weighted mean $^{206}Pb/^{238}U$ age of 522.4±2.0 Ma using both single- and multi-grain U-Pb ID-TIMS techniques Landing et al. (1998); Compston et al. (1992). In M236, six grains subjected to chemical abrasion form a cluster with a weighted mean $^{206}Pb/^{238}U$ date of 520.93±0.14 Ma (MSWD = 0.42), which we interpret as the eruption/depositional age (Table DR1).

TABLE S1. U-Pb isotopic data for zircon analyzed from early Cambrian volcanic ashes of Morocco

							Ratios						Ages (Ma)			
Sample		Pb_c	Pb*	Th	^{206}Pb	^{208}Pb	^{206}Pb	err	^{207}Pb	err	^{207}Pb	err	^{206}Pb	^{207}Pb	^{207}Pb	corr.
Fractions		(pg)	Pb_c	U	^{204}Pb	^{206}Pb	^{238}U	(2σ%)	^{235}U	(2σ%)	^{206}Pb	(2σ%)	^{238}U	^{235}U	^{206}Pb	coef.
(a)		(b)	(b)		(c)	(d)	(e)		(e)		(e)					
M223 - Adoudou Formation																
z1*	aa	2.3	134.6	0.29	8512.1	0.091	0.084901	(.05)	0.67840	(.10)	0.05795	(.09)	**525.31**	**525.80**	**528.0**	0.532
z2*	aa	0.7	442.4	0.33	27652	0.103	0.084893	(.06)	0.67828	(.08)	0.05795	(.05)	**525.26**	**525.73**	**527.8**	0.773
z3*	aa	1.2	96.9	0.32	6082.4	0.101	0.084897	(.06)	0.67855	(.15)	0.05797	(.13)	**525.29**	**525.90**	**528.6**	0.520
z4*	aa	1.3	91.7	0.35	5706.7	0.110	0.084611	(.09)	0.67631	(.16)	0.05797	(.13)	**523.58**	**524.54**	**528.7**	0.609
z7*	aa	1.2	55.4	0.31	3488.8	0.099	0.084908	(.06)	0.67883	(.20)	0.05798	(.18)	**525.35**	**526.06**	**529.1**	0.470
z8*	aa	0.6	71.6	0.29	4535.2	0.091	0.084884	(.08)	0.67853	(.20)	0.05798	(.17)	**525.21**	**525.89**	**528.8**	0.497
z9*	ca	0.4	97.7	0.33	6106.9	0.105	0.084904	(.05)	0.67842	(.14)	0.05795	(.12)	**525.33**	**525.82**	**527.9**	0.453
z10*	ca	0.4	112.7	0.34	7032.2	0.107	0.084905	(.05)	0.67832	(.15)	0.05794	(.13)	**525.33**	**525.76**	**527.6**	0.451
z11*	ca	0.6	85.6	0.32	5381.0	0.100	0.084929	(.06)	0.67859	(.15)	0.05795	(.13)	**525.48**	**525.92**	**527.8**	0.519
z12	ca	1.0	20.9	0.31	1329.0	0.097	0.084896	(.07)	0.67950	(.50)	0.05805	(.46)	**525.28**	**526.47**	**531.6**	0.595
z13	ca	0.4	64.4	0.34	4023.2	0.108	0.084907	(.06)	0.67886	(.20)	0.05799	(.18)	**525.34**	**526.09**	**529.3**	0.437
z14	ca	0.5	68.0	0.32	4272.2	0.100	0.084937	(.06)	0.67909	(.18)	0.05799	(.16)	**525.53**	**526.22**	**529.3**	0.460
M231 - Adoudou Formation																
z1	aa	0.3	345.6	0.55	20368	0.173	0.084840	(.04)	0.67724	(.08)	0.05789	(.06)	**524.95**	**525.10**	**525.8**	0.599
z2	aa	0.3	350.0	0.55	20622	0.173	0.084839	(.05)	0.67725	(.08)	0.05790	(.06)	**524.94**	**525.11**	**525.8**	0.621
z3	aa	0.4	214.3	0.55	12634	0.173	0.084852	(.07)	0.67726	(.11)	0.05789	(.08)	**525.02**	**525.12**	**525.5**	0.660
z4	aa	0.3	321.3	0.51	19143	0.160	0.084818	(.05)	0.67701	(.08)	0.05789	(.07)	**524.82**	**524.97**	**525.6**	0.578
z5	aa	0.3	297.8	0.54	17620	0.168	0.084797	(.05)	0.67706	(.08)	0.05791	(.06)	**524.69**	**525.00**	**526.3**	0.587
z6	ca	0.4	79.8	0.49	4788.6	0.154	0.084761	(.05)	0.67708	(.17)	0.05793	(.15)	**524.48**	**525.01**	**527.3**	0.452
z7	ca	0.6	56.5	0.51	3383.2	0.159	0.084794	(.08)	0.67690	(.27)	0.05790	(.24)	**524.67**	**524.90**	**525.9**	0.450
z8	ca	0.4	131.1	0.54	7757.5	0.170	0.084809	(.05)	0.67732	(.12)	0.05792	(.11)	**524.76**	**525.15**	**526.8**	0.495
z9	ca	0.4	190.1	0.50	11360	0.157	0.084818	(.05)	0.67731	(.10)	0.05792	(.09)	**524.82**	**525.15**	**526.6**	0.507
M234 - Lie de Vin Formation																
z1	ca	0.5	27.4	0.34	1721.5	0.106	0.084509	(.08)	0.67478	(.45)	0.05791	(.42)	**522.98**	**523.62**	**526.4**	0.473
z2	ca	0.5	40.8	0.44	2491.3	0.139	0.084522	(.06)	0.67475	(.29)	0.05790	(.27)	**523.06**	**523.60**	**525.9**	0.470
z3	ca	0.5	28.8	0.36	1799.9	0.115	0.084667	(.07)	0.67765	(.39)	0.05805	(.37)	**523.92**	**525.36**	**531.6**	0.480
z4	ca	0.5	41.9	0.35	2622.9	0.108	0.084552	(.07)	0.67402	(.29)	0.05782	(.26)	**523.23**	**523.15**	**522.8**	0.454
z5	ca	0.5	20.8	0.29	1331.4	0.093	0.084611	(.09)	0.67682	(.52)	0.05802	(.48)	**523.59**	**524.85**	**530.3**	0.490
z6	ca	0.5	29.2	0.48	1767.1	0.151	0.084488	(.09)	0.67480	(.41)	0.05793	(.38)	**522.85**	**523.63**	**527.0**	0.457
z7	ca	0.4	50.0	0.54	2971.5	0.169	0.084543	(.07)	0.67476	(.27)	0.05789	(.25)	**523.18**	**523.61**	**525.5**	0.444
z8	ca	0.4	41.2	0.45	2511.1	0.140	0.084577	(.06)	0.67515	(.28)	0.05790	(.26)	**523.38**	**523.84**	**525.8**	0.465
z10	ca	0.3	25.6	0.50	1544.8	0.158	0.084584	(.16)	0.67548	(.71)	0.05792	(.66)	**523.42**	**524.04**	**526.7**	0.390
z11	ca	0.3	37.2	0.64	2159.3	0.202	0.084481	(.10)	0.67426	(.39)	0.05789	(.36)	**522.81**	**523.30**	**525.4**	0.415
z12	ca	0.3	10.0	0.48	618.2	0.151	0.084603	(.18)	0.67478	(1.25)	0.05785	(1.16)	**523.54**	**523.62**	**523.9**	0.497
M236 - Lie de Vin Formation																
z1	ca	0.6	31.7	0.34	1991.2	0.106	0.084172	(.07)	0.67121	(.37)	0.05783	(.35)	**520.98**	**521.45**	**523.5**	0.469
z2	ca	0.7	81.5	0.46	4933.0	0.144	0.084143	(.06)	0.67087	(.18)	0.05783	(.16)	**520.81**	**521.24**	**523.1**	0.449
z3	ca	0.6	34.6	0.53	2059.8	0.168	0.090252	(.06)	0.73314	(.33)	0.05892	(.31)	**557.03**	**558.40**	**564.0**	0.499
z4	ca	0.6	13.9	0.40	867.6	0.126	0.084205	(.10)	0.67191	(.88)	0.05787	(.81)	**521.17**	**521.88**	**525.0**	0.651
z5	ca	0.9	8.8	0.79	487.3	0.229	0.377095	(.83)	6.68588	(1.11)	0.12859	(.64)	**2062.7**	**2070.8**	**2078.8**	0.818
z6	ca	0.7	52.8	0.38	3267.5	0.120	0.084323	(.11)	0.67278	(.33)	0.05787	(.30)	**521.87**	**522.40**	**524.7**	0.447
z7	ca	0.5	21.0	0.36	1318.3	0.112	0.084171	(.08)	0.67112	(.52)	0.05783	(.48)	**520.97**	**521.39**	**523.2**	0.550
z8	ca	0.4	74.7	0.36	4645.4	0.112	0.084171	(.05)	0.67160	(.17)	0.05787	(.15)	**520.97**	**521.68**	**524.8**	0.457
z9	ca	0.6	84.8	0.35	5277.5	0.111	0.084147	(.07)	0.67179	(.17)	0.05790	(.14)	**520.83**	**521.80**	**526.0**	0.515

Notes: Corr. coef. = correlation coefficient. Age calculations are based on the decay constants of Jaffey et al. (1971).

(a) All analyses are single zircon grains pre-treated by either the thermal annealing and acid leaching technique (ca) or air abrasion (aa). Data used in age calculations are in bold. * denotes data from Maloof et al. (2005) recalculated with new tracer calibration.

(b) Pb_c is total common Pb in analysis. Pb* is radiogenic Pb concentration.

(c) Measured ratio corrected for spike and fractionation only.

(d) Radiogenic Pb ratio.

(e) Corrected for fractionation, spike, blank, initial common Pb and Th disequilibrium. Mass fractionation correction of 0.25%/amu ± 0.04%/amu (atomic mass unit) was applied to single-collector Daly analyses. Total procedural blank normally less than 1.0 pg for Pb and less than 0.1 pg for U. Blank isotopic composition: $^{206}Pb/^{204}Pb$ = 18.31 ± 0.53, $^{207}Pb/^{204}Pb$ =15.38 ± 0.35, $^{208}Pb/^{204}Pb$ = 37.45 ± 1.1.

Table DR1

Supplementary Online Materials: U/Pb zircon data table.

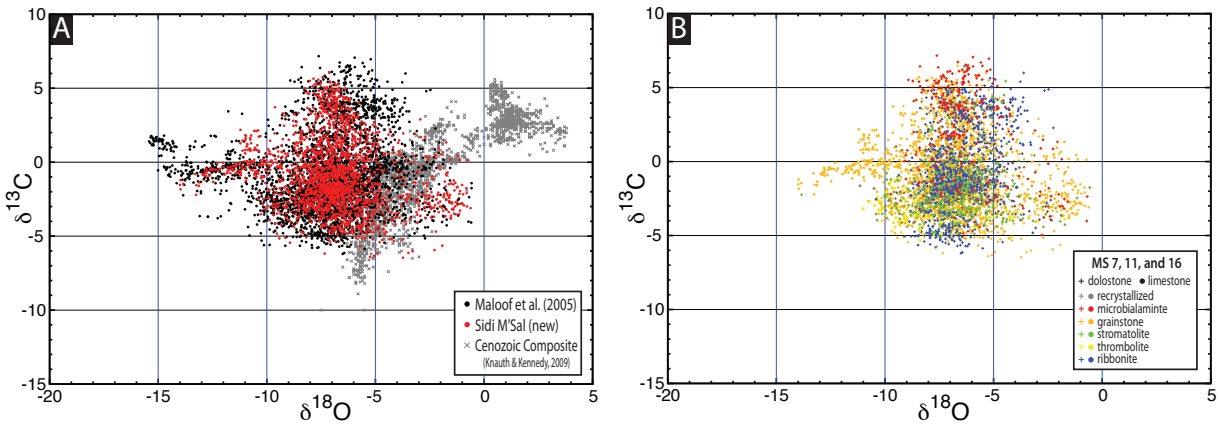

Figure DR1. **Supplementary Online Materials: $\delta^{18}O$ – $\delta^{13}C$ cross plots. In (A), all Morocco data from Maloof et al. (2005) are plotted in black, while new data from Sidi M'Sal are plotted in red. For reference, Cenozoic carbonate platform data compiled by Knauth and Kennedy Knauth and Kennedy (2009) from the Bahamas Melim et al. (2001) and Enewetak Atoll Quinn (1990) are plotted with grey x's. In (B), we plot data only from Oued Sdas (MS7), Zawyat n' Bougzoul (MS11) and Sidi M'Sal (MS16) and we differentiate between dolostone (+'s) and limestone (circles) and between the carbonate lithofacies (colors) depicted in Fig. 2. Specimen that are so recrystallized that their lithofacies are uncertain are plotted in grey.**

References

Banner, J. and Hanson, G., 1990, Calculation of simultaneous isotopic and trace element variations during water-rock interaction with applications to carbonate diagenesis: Geochimica Cosmochimicha Acta, vol. 54, pp. 3123–3137.

Compston, W., Williams, I., Kirschvink, J., Zichao, Z., and Guogan, M., 1992, Zircon U-Pb ages from the Early Cambrian time-scale: Journal of the Geological Society of London, vol. 149, pp. 171–184.

Jaffey, A., Flynn, K., Glendenin, L., Bentley, W., and Essling, A., 1971, Precision measurement of half-lives and specific activities of ^{235}U and ^{238}U: Physical Review, vol. C4, pp. 1889–1906.

Knauth, L. and Kennedy, M., 2009, The late Precambrian greening of the Earth: Nature, vol. 460, pp. 728–731.

Krogh, T., 1973, A low contamination method for the hydrothermal decomposition of zircon and extraction of U and Pb for isotopic age determinations: Geochimica Cosmochimicha Acta, vol. 37, pp. 485–494.

Landing, E., Bowring, S., Davidek, K., Westrop, S., Geyer, G., and Heldmaier, W., 1998, Duration of the Early Cambrian: U-Pb ages of volcanic ashes from Avalon and Gondwana: Canadian Journal of Earth Science, vol. 35, pp. 329–338.

Ludwig, K., 1980, Calculation of uncertainties of U-Pb isotope data: Earth and Planetary Science Letters, vol. 46, pp. 212–220.

Ludwig, K., 2005, Isoplot/Ex. V. 3: USGS, vol. Open-File Report.

Maloof, A., Schrag, D., Crowley, J., and Bowring, S., 2005, An expanded record of early cambrian carbon cycling from the anti-atlas margin, morocco: Canadian Journal of Earth Science, vol. 42, pp. 2195–2216.

Mattinson, J., 2000, Revisiting the "gold standard" - the uranium decay constants of Jaffey et al., 1971: Eos Transactions of the American Geophysical Union, Spring Meeting Supplement, vol. 81, pp. V61A–02.

Mattinson, J., 2005, Zircon U-Pb chemical abrasion (“CA-TIMS”) method: combined annealing and multi-step partial dissolution analysis for improved precision and accuracy of zircon ages: Chemical Geology, vol. 220, pp. 47–66.

Melim, L., Swart, P., and Maliva, R., 2001, Meteoric and marine-burial diagenesis in the subsurface of the Great Bahama Bank: *In* Ginsburg, R., ed., Subsurface Geology of a prograding carbonate platform margin, Great Bahama Bank: Results of the Bahamas Drilling Project, SEPM.

Patterson, W. and Walter, L., 1994, Depletion of ^{13}C in seawater σCO_2 on modern carbonate platformsl Significance for the carbon isotopic record of carbonates: Geology, vol. 22, pp. 885–888.

Quinn, T., 1990, Meteoric diagenesis of Plio-Pleistocene limestones at Enewetak Atoll: Journal of Sedimentary Petrology, vol. 61, pp. 681–703.

Ramezani, J., Schmitz, M., Davydov, V., Bowring, S., Snyder, W., and Northrup, C., 2007, High-precision

U-Pb zircon age constraints on the Carboniferous-Permian boundary in the Southern Urals stratotype: Earth Planet. Sci. Lett., vol. 256, pp. 244–257.

Schoene, B., Crowley, J., Condon, D., Schmitz, M., and Bowring, S., 2006, Reassessing the uranium decay constants for geochronology using ID-TIMS U-Pb data: Geochimica Cosmochimicha Acta, vol. 70, pp. 426–445.

Swart, P., 2008, Global synchronous changes in the carbon isotopic composition of carbonate sediments unrelated to changes in the global carbon cycle: Proc. Nat. Acad. Sci., vol. 105, pp. 13,741–13,745.

Swart, P. and Eberli, G., 2005, The nature of the $\delta^{13}C$ of periplatform sediments: Implications for stratigraphy and the global carbon cycle: Sedimentary Geology, vol. 175, pp. 115–129.